

See discussions, stats, and author profiles for this publication at: <https://www.researchgate.net/publication/276238372>

# Solid-State Reaction Synthesis of a InSe/CuInSe<sub>2</sub> Lateral p-n Heterojunction and Application in High Performance Optoelectronic Devices

ARTICLE in CHEMISTRY OF MATERIALS · JANUARY 2015

Impact Factor: 8.35 · DOI: 10.1021/cm504268j

---

READS

29

## 6 AUTHORS, INCLUDING:



Guangbo Liu

Harbin Institute of Technology

8 PUBLICATIONS 39 CITATIONS

[SEE PROFILE](#)



Wenwu Cao

Pennsylvania State University

462 PUBLICATIONS 6,574 CITATIONS

[SEE PROFILE](#)

# Solid-State Reaction Synthesis of a InSe/CuInSe<sub>2</sub> Lateral p–n Heterojunction and Application in High Performance Optoelectronic Devices

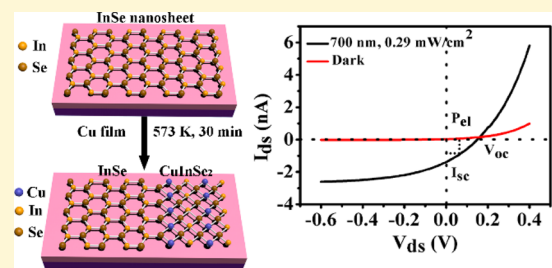
Wei Feng,<sup>†,‡</sup> Wei Zheng,<sup>†</sup> XiaoShuang Chen,<sup>†</sup> Guangbo Liu,<sup>†</sup> Wenwu Cao,<sup>§</sup> and PingAn Hu<sup>\*,†</sup>

<sup>†</sup>Key Lab of Microsystem and Microstructure of Ministry of Education and <sup>‡</sup>School of Materials Science and Engineering, Harbin Institute of Technology, No. 2 Yi Kuang Street, Harbin, 150080, China

<sup>§</sup>Department of Mathematics and Materials Research Institute, The Pennsylvania State University, University Park, Pennsylvania 16802, United States

## Supporting Information

**ABSTRACT:** Graphene-like layered semiconductors are a new class of materials for next generation electronic and optoelectronic devices due to their unique electrical and optical properties. A p–n junction is an elementary building block for electronics and optoelectronics devices. Here, we demonstrate the fabrication of a lateral p–n heterojunction diode of a thin-film InSe/CuInSe<sub>2</sub> nanosheet by simple solid-state reaction. We discover that InSe nanosheets can be easily transformed into CuInSe<sub>2</sub> thin film by reacting with elemental copper at a temperature of 300 °C. Photodetectors and photovoltaic devices based on this lateral heterojunction p–n diode show a large photoresponsivity of 4.2 A W<sup>-1</sup> and a relatively high light-power conversion efficiency of 3.5%, respectively. This work is a giant step forward in practical applications of two-dimensional materials for next generation optoelectronic devices.



## INTRODUCTION

The quest for next generation electronics, photodetectors, and photovoltaic devices as well as sensors and displays necessitates the development and exploration of a new class of high performance materials with superior electronic and optoelectronic properties. Graphene-like two-dimensional (2D) semiconductors, such as monolayer or few-layer MoS<sub>2</sub>,<sup>1</sup> WSe<sub>2</sub>,<sup>2,3</sup> InSe,<sup>4,5</sup> black phosphorus,<sup>6,7</sup> etc., have atomic flatness and novel thickness dependent quantum confinement properties. Their easier production in large areas and low cost make them attractive for future flexible, miniaturized, and high performance electronic and optoelectronic devices.<sup>8</sup> Recently, new optoelectronic devices have been demonstrated using various thin layered semiconductors of MoS<sub>2</sub>,<sup>9,10</sup> WSe<sub>2</sub>,<sup>11</sup> MoSe<sub>2</sub>,<sup>12</sup> GaSe,<sup>13</sup> GaS,<sup>14</sup> InSe,<sup>5,15</sup> and black phosphorus<sup>16</sup> and show much superior performance than devices made of conventional amorphous and polycrystalline materials.

The p–n junction is a basic building block of many electronic and optoelectronic devices, including diodes, photodetectors, and solar cells. Recently, a p–n junction diode has been realized in ionic liquid gated multilayer MoS<sub>2</sub>,<sup>17</sup> but the device must be operated at 180 K or below, which limits its practical applications. Vertical p–n heterojunctions based on 2D/thin-film TMDs have been demonstrated.<sup>18–24</sup> Lateral p–n junctions in monolayer WSe<sub>2</sub><sup>25,26</sup> or few-layer black phosphorus<sup>27</sup> induced by electrostatic gating operation within multigate device configurations have been demonstrated for applications in photodetectors, photovoltaic devices, and light-emitting

diodes.<sup>25–27</sup> Monolayer WSe<sub>2</sub> p–n junctions based optoelectronic devices exhibit poor performance, including a low photoresponsivity of 210 mA W<sup>-1</sup> in photodetectors and low light-power conversion efficiency of 0.5% in photovoltaic devices,<sup>25,26</sup> due to the chosen imperfect contact metals.<sup>11</sup> Moreover, multigate device configurations require complex and specialized fabrication procedures that are not compatible with current semiconductor fabrication technology. Besides, this method is only suitable for monolayer or few-layer materials because electrical properties of thicker film materials cannot be sufficiently controlled by electrostatic gating due to screening effects.<sup>27</sup> In order to work as a p–n diode, external gate voltage must be applied to drive these devices, which limits them in practical applications. Lateral heterojunctions within monolayer MoSe<sub>2</sub>–WSe<sub>2</sub> have been grown by lateral heteroepitaxy using physical vapor transport, which allows new device functionalities, such as in-plane transistors and diodes, to be integrated within a 2D heterojunction.<sup>28</sup>

Unlike indirect band gap multilayer transition metal dichalcogenides (TMDs) of MoS<sub>2</sub> and WSe<sub>2</sub>, multilayer InSe possesses a direct band gap, low effective mass,<sup>29</sup> and high electron mobility<sup>30</sup> so that it has been applied in high performance photodetectors.<sup>5</sup> Copper indium diselenide (CuInSe<sub>2</sub>) is an important gallium diselenide (CIGS) solar

Received: November 20, 2014

Revised: January 19, 2015

Published: January 20, 2015

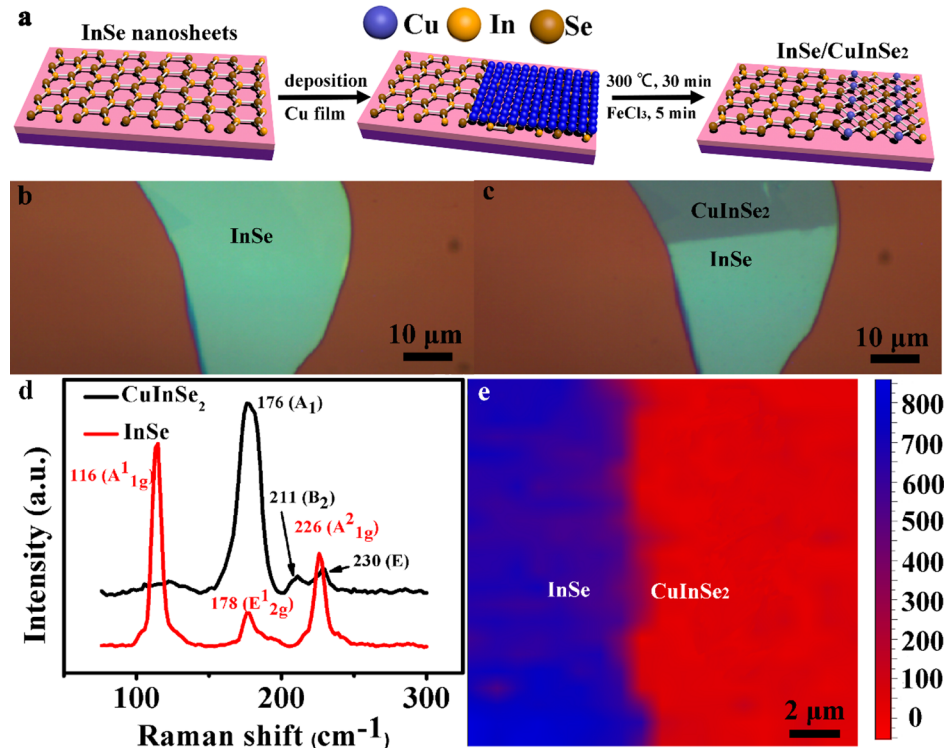


**Figure 1.** (a) Synthesis schematic for InSe/CuInSe<sub>2</sub> lateral heterojunction nanosheets. (b) Optical image of InSe nanosheets on a 285 nm SiO<sub>2</sub>/Si substrate. (c) Optical image of fabricated lateral InSe/CuInSe<sub>2</sub> heterojunction. (d) Raman patterns of InSe/CuInSe<sub>2</sub> heterojunction nanosheets. (e) Raman mapping (InSe A<sup>1</sup><sub>1g</sub> peak of 116 cm<sup>-1</sup>) of the interface of the InSe/CuInSe<sub>2</sub> heterojunction. The wavelength and intensity of the laser used for Raman spectroscopy are 532 nm and 1 mW, respectively.

energy material, which exhibits effective light-absorbing capability due to its direct band gap of 1.1 eV and high optical absorption coefficient.<sup>31</sup> A possible way to obtain high quality CuInSe<sub>2</sub> nanowires and nanosheets using the as-grown In<sub>2</sub>Se<sub>3</sub> nanowires<sup>32</sup> and as-exfoliation In<sub>2</sub>Se<sub>3</sub> nanosheets<sup>33</sup> as a template to react with the copper element has been demonstrated.<sup>32–34</sup> Though the In<sub>2</sub>Se<sub>3</sub>/CuInSe<sub>2</sub> nanoheterostructures also have been constructed by solid state reactions,<sup>35</sup> the electronic and optoelectronic devices based on In<sub>2</sub>Se<sub>3</sub>/CuInSe<sub>2</sub> nanoheterostructures have not been demonstrated. Recently, multilayer InSe photodetectors on rigid and flexible substrates show broadband photodetection from the visible to near-infrared region with high responsivity.<sup>15,36</sup> The room temperature carrier mobility of the multilayer InSe transistor can be enhanced up to 1055 cm<sup>2</sup> V<sup>-1</sup> s<sup>-1</sup> through the suppression of carrier scattering from chemical impurities at oxidized dielectric.<sup>37</sup>

Chemical doping by the introduction of additional elements into the semiconductor is a powerful and facile approach for modulating electronic and optoelectronic properties, which is widely used in bulk semiconductor processing and just has been realized in p–n junction fabrication in thin layered semiconductors.<sup>38</sup> In this work, we have succeeded in the fabrication of a lateral thin-film InSe/CuInSe<sub>2</sub> p–n heterojunction by a simple chemical doping procedure. Furthermore, we demonstrate the application of this lateral p–n heterojunction in high performance optoelectronics to obtain a high photoresponsivity of 4.2 A W<sup>-1</sup> for photodetectors and relatively high power conversion efficiency of 3.5% for photovoltaic devices. These exciting results pave the way for practical optoelectronic and electronic applications of InSe/CuInSe<sub>2</sub> heterojunctions.

## ■ EXPERIMENTAL SECTION

**Synthesis and Characterization of InSe/CuInSe<sub>2</sub> Heterojunction Nanosheets.** Multilayer InSe nanosheets were mechanically exfoliated from bulk InSe crystals using scotch tape. The pieces of scotch tape with InSe nanosheets were put on silicon substrate coated with 285 nm SiO<sub>2</sub>. Then scotch tape pieces were taken away, and the InSe nanosheets were transferred onto the substrate. The thickness was determined by using atomic force microscopy (AFM, Nanoscope IIIa Vecco). Then suitable InSe nanosheets (thickness: 20–50 nm, length: 30–50 μm, width: 15–30 μm) were identified using an optical microscope, and half of the sheets' areas were masked by Cu film using thermal evaporation. These copper coated nanosheets were annealed in a tube furnace at 573 K for 30 min with 100 sccm of Ar. After annealing, the residual Cu on the nanosheets was removed by a simple cleaning step of 5 min submersion in 3 M aqueous FeCl<sub>3</sub>. The structure and composition of InSe/CuInSe<sub>2</sub> heterojunction nanosheets were identified by Raman spectroscopy (LabRAM XploRA, laser wavelength is 532 nm and power is 1 mW) and transmission electron microscopy (Tecnai-G2 F30, accelerating voltage of 300 kV) attached with an energy-dispersive X-ray spectroscopy (EDS).

**Fabrication of InSe/CuInSe<sub>2</sub> Diodes and Characterizations of Electronic and Optoelectronic Properties of InSe/CuInSe<sub>2</sub> Diodes.** The lateral InSe/CuInSe<sub>2</sub> heterojunction p–n diodes (thickness: 20–50 nm, length: 30–50 μm, width: 15–30 μm) were fabricated by metal thermal evaporation with copper mask. Cr/Au electrodes with 5 nm thick Cr and 35 nm thick Au were evaporated onto the nanosheets. Electrical characterizations of p–n diode based on InSe/CuInSe<sub>2</sub> heterojunction were performed by using a semiconductor characterization system (Keithley 4200 SCS) with a Lakeshore probe station. Monochromatic lights of 254–850 nm were obtained by using optical filters using a 500 W xenon lamp as the light source. The photocurrent measurements were performed by the semiconductor characterization system (Keithley 4200 SCS) with a Lakeshore probe station. The intensities of incident light source were measured by a power and energy meter (Model 372, Scientech).

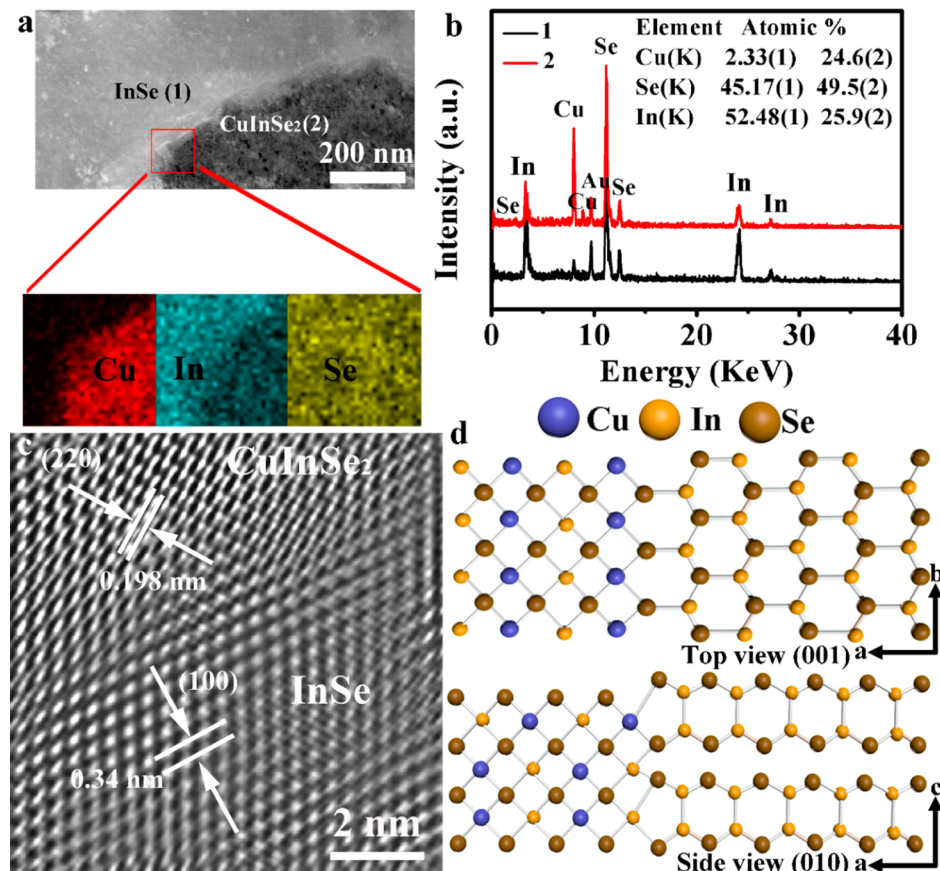
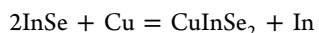


**Figure 2.** Structure characterization of InSe/CuInSe<sub>2</sub> heterojunction. (a) A typical TEM images of 2D InSe/CuInSe<sub>2</sub> heterojunction nanosheets at low magnification; bottom image is element distribution mapping. (b) The EDS images of InSe and CuInSe<sub>2</sub> heterojunction. (c) A typical HRTEM image of the interface of InSe/CuInSe<sub>2</sub> heterojunction nanosheets. (d) Top view (corresponding to (001) plane, top image) and side view (corresponding to (010) plane, bottom image) crystal structure of InSe/CuInSe<sub>2</sub> heterojunction.

## RESULTS AND DISCUSSION

**Synthesis and Characterizations of InSe/CuInSe<sub>2</sub> Heterojunction Nanosheets.** InSe is a typical layered semiconductor with hexagonal structure, and CuInSe<sub>2</sub> is a nonlayered semiconductor with chalcopyrite structure. The hexagonal layered InSe can transformed to chalcopyrite nonlayered CuInSe<sub>2</sub> with copper film via solid-state reaction:



The entire process of fabricating thin film InSe/CuInSe<sub>2</sub> p–n heterojunctions by chemical doping via solid-state reaction is illustrated in Figure 1a (more details can be found in the Experimental Section). In order to fabricate InSe/CuInSe<sub>2</sub> p–n heterojunction in one nanosheet, the partial area of InSe is transformed into CuInSe<sub>2</sub> while the other part should be unchanged. So half the area of the InSe nanosheets is masked by Cu film using thermal evaporation (Figure 1a, middle image). The partial color contrast change of the InSe sheet in Figure 1b indicates that some regions of layered InSe nanosheet are transformed into nonlayered CuInSe<sub>2</sub> after annealing with covered copper film. The overall morphology of the heterojunction nanosheet (Figure 1c) remains unchanged in comparison to the starting InSe nanosheet (Figure 1b).

In order to confirm that the InSe/CuInSe<sub>2</sub> heterojunction has been formed, Raman characterizations are performed. Raman spectrum taken from the copper doping region (Figure 1d) shows three new peaks of strong A<sub>1g</sub>, 176 cm<sup>-1</sup>; weak B<sub>2g</sub>,

211 cm<sup>-1</sup>; and E, 230 cm<sup>-1</sup> and is primarily indexed to CuInSe<sub>2</sub><sup>39</sup> which is totally different from InSe Raman spectra of A<sub>1g</sub>, 116 cm<sup>-1</sup>; E<sub>1g</sub>, 178 cm<sup>-1</sup>; and A<sub>2g</sub>, 226 cm<sup>-1</sup>, suggesting the copper covered region of InSe nanosheet completely transforms into CuInSe<sub>2</sub>. Figure 1e shows the Raman mapping (InSe: A<sub>1g</sub> peak of 116 cm<sup>-1</sup>) of the interface of the InSe/CuInSe<sub>2</sub> heterojunction. The CuInSe<sub>2</sub> is homogeneously distributed on the copper covered part, and the InSe/CuInSe<sub>2</sub> interface is clearly visible. The Raman mapping has revealed that layered InSe and nonlayered CuInSe<sub>2</sub> can coexist in the same nanosheet and the boundary between the two materials is sharp.

The microstructure and spatial distribution of elemental composition of the InSe/CuInSe<sub>2</sub> heterojunction are investigated using transmission electron microscopy (TEM) combined with energy-dispersive X-ray spectroscopy (EDS). Figure 2a shows a typical TEM image of the InSe/CuInSe<sub>2</sub> heterojunction. The bottom image is detected Cu, In, and Se elemental mapping of a selected region of this heterojunction (marked with a red rectangle in Figure 2a, top image). As can be seen, In and Se elements are homogeneously distributed over the whole nanosheet, while Cu is located mainly on one side. The lateral InSe/CuInSe<sub>2</sub> heterostructure is also confirmed by elemental analysis. Figure 2b is the EDS spectra collected from two different positions along the direction of the interface of the heterojunction, which reveals that the position 2 is composed of considerable Se, Cu, and In with an atomic ratio of 1:1:2 (CuInSe<sub>2</sub>), while position 1 mainly consists of Se and

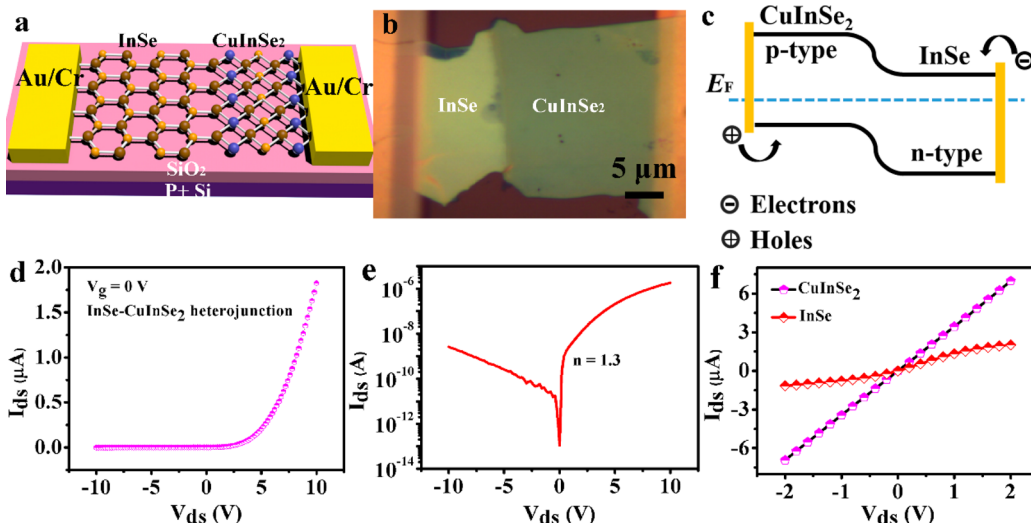


**Figure 3.** Electrical characteristics of InSe/CuInSe<sub>2</sub> lateral heterojunction diode. (a) Cross-sectional schematic of InSe/CuInSe<sub>2</sub> lateral heterojunction diode device. (b) Optical image of a representative InSe/CuInSe<sub>2</sub> lateral heterojunction diode. (c) Schematic energy band diagram of the diode. Electrons are injected from n-type InSe, and holes are injected from the p-type CuInSe<sub>2</sub>. (d) Representative linear  $I$ – $V$  characteristic of InSe/CuInSe<sub>2</sub> diode. (e) Corresponding semilogarithmic plot of the  $I$ – $V$  curve. (f) Representative  $I$ – $V$  characteristic of InSe and CuInSe<sub>2</sub> nanosheets devices measured under  $V_g = 0$  V.

In elements with negligible Cu element (the detected Au and C elements originate from the microgrid), which is consistent with the element mappings. Figure 2c shows the high-resolution TEM (HRTEM) image measured from the interface region of the heterojunction, which shows both crystalline InSe and CuInSe<sub>2</sub> regions in the same nanosheet, and the result is in good agreement with the previous structural and compositional characterizations (Figure 2a,b); it further confirms the successful formation of a lateral heterojunction. It is obvious that starting InSe has a hexagonal structure, while synthesis CuInSe<sub>2</sub> has a chalcopyrite structure as shown in HRTEM (along the  $\langle 001 \rangle$  zone axis). The measured lattice spacing of 0.198 nm corresponds to the (220) plane of CuInSe<sub>2</sub>,<sup>34</sup> and the lattice spacing of 0.34 nm corresponds to the (100) plane of InSe.<sup>37</sup> Figure 2d shows the ideal crystal structure of InSe/CuInSe<sub>2</sub> heterojunction from the top view ((001) plane, which corresponds to the HRTEM image) and side view ((010) plane). The hexagonal layered InSe and chalcopyrite non-layered CuInSe<sub>2</sub> are connected by Cu–Se and In–Se bonds as shown in the crystal structure. There is a transition zone between InSe and CuInSe<sub>2</sub> phases as shown in the HRTEM image, which can be attributed to diffusion of Cu in InSe upon annealing. We find that the quality of less than 10 nm thick CuInSe<sub>2</sub> sheets prepared by this process will degrade significantly and may even form noncontinuous films (Supporting Information Figure S3). So in this study, we pay attention to InSe/CuInSe<sub>2</sub> with a thickness range of 20–50 nm. The AFM images of the CuInSe<sub>2</sub> nanosheet reveal that the surface of the CuInSe<sub>2</sub> nanosheet is rough as shown in Supporting Information Figures S2 and S3c. The rough surface and defects can be ascribed to two following reasons: (1) The CuInSe<sub>2</sub> nanosheets are synthesized by solid-state reaction at 573 K for 30 min. The reaction temperature will aggravate lattice vibration and introduce roughness and some defects. (2) The solid-state reaction is a replacement reaction: The generated In will escape from nanosheets and also produce some defects.

#### Fabrication and Electronic Characterizations of InSe/CuInSe<sub>2</sub> Diodes.

To reveal the intrinsic electronic properties

of InSe/CuInSe<sub>2</sub>, we fabricated three electronic devices on the SiO<sub>2</sub>/Si substrate using thin-film of multilayer InSe, CuInSe<sub>2</sub>, and InSe/CuInSe<sub>2</sub> heterojunction, respectively (see detailed information in the Experimental Section). The multilayer InSe and thin-film CuInSe<sub>2</sub> are determined to be n- and p-type semiconductors by electrically measuring their corresponding field effect transistor (FETs) as shown in Supporting Information Figure S1. The mobilities of multilayer InSe and thin-film CuInSe<sub>2</sub> FET are  $62 \text{ cm}^2 \text{ V}^{-1} \text{ s}^{-1}$  and  $1.2 \text{ cm}^2 \text{ V}^{-1} \text{ s}^{-1}$ , respectively. The performance of thin-film CuInSe<sub>2</sub> FET is poor due to the surface roughness and defects generating from the synthesis process. The 3D schematic of InSe/CuInSe<sub>2</sub> p–n diode is shown in Figure 3a. A typical optical image of the device is shown in Figure 3b, and the width and length are 15 and 30  $\mu\text{m}$ , respectively. The thickness of the channels used in our study is in the range of 20 to 50 nm. An AFM image of a typical 40 nm channel InSe/CuInSe<sub>2</sub> p–n diode is shown in Supporting Information Figure S2. Thinner sheet heterojunctions (<10 nm) exhibit significantly degraded film quality and poor performance, e.g., a weaker diode behavior was observed in ~11 nm thick InSe/CuInSe<sub>2</sub>, in which the CuInSe<sub>2</sub> part is a rough and segmented film (Supporting Information Figure S3).

The electrostatic coupling between metal electrodes and the Si gate can affect the properties of the InSe/CuInSe<sub>2</sub> p–n heterojunction diode. In order to eliminate the electrostatic coupling and reveal intrinsic electronic and optoelectronic properties of InSe/CuInSe<sub>2</sub> p–n heterojunction diode, devices are measured using a two-probe structure without a Si gate. We propose the energy band diagrams of InSe/CuInSe<sub>2</sub> p–n heterojunction diode in Figure 3c, forming typical type-II band alignment. A representative  $I$ – $V$  characteristic of the InSe/CuInSe<sub>2</sub> heterojunction diode is shown in Figure 3d, showing robust rectifying behavior with a current of  $1.8 \mu\text{A}$  at a forward bias of 10 V. The ideality factor can be deduced from the Shockley diode equation:  $I = I_s(\exp(V_{ds}/nV_T) - 1)$ , where  $I_s$  is the reverse bias current,  $n$  is the ideality factor, and  $V_T$  is the thermal voltage. The value of  $n$  can be calculated to be 1.3 using the rapid increase of current at forward bias as shown in Figure

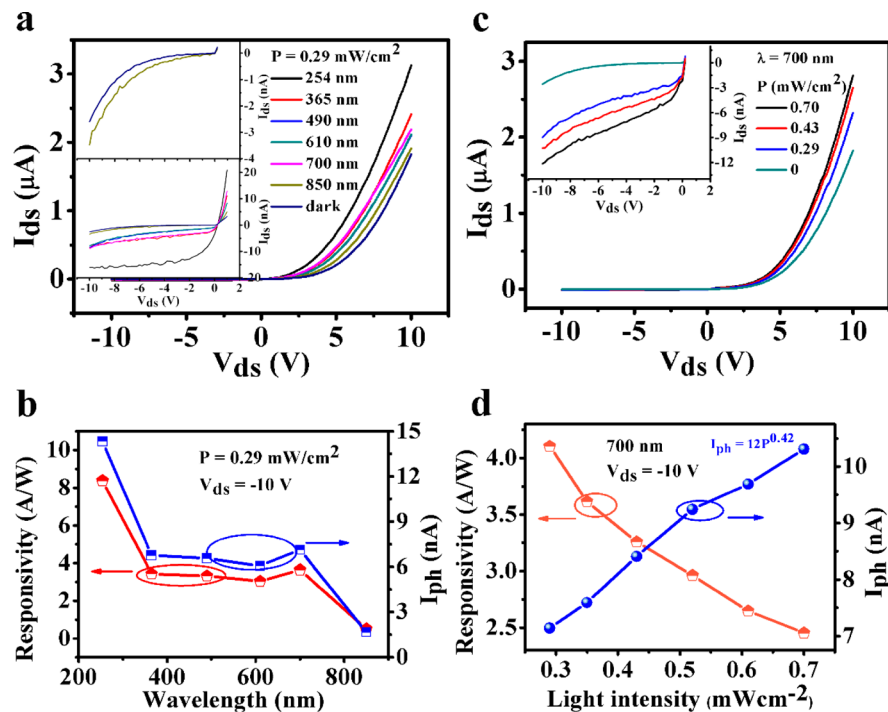


**Figure 4.** Device operation as photodetector. (a)  $I$ – $V$  characterizations of InSe/CuInSe<sub>2</sub> diode under various illumination wavelengths at 0.29 mW cm<sup>−2</sup>. Inset: upper is the enlarged  $I$ – $V$  curves of diode applied reverse bias voltages under 850 nm illumination, bottom is the enlarged  $I$ – $V$  curves of diode applied reverse bias voltages under various illumination wavelengths as a photodetector. (b) Photocurrent and responsivity as a function of various illumination wavelengths under  $V_{ds} = -10$  V extracted from data shown in (a). (c)  $I$ – $V$  characterizations of InSe/CuInSe<sub>2</sub> diode under 700 nm optical illumination with various intensities; Inset is the enlarged  $I$ – $V$  curves of diode applied reverse bias voltages with 700 nm optical illumination with various intensities as a photodetector. (d) Photocurrent and responsivity as a function of optical intensity under  $V_{ds} = -10$  V extracted from data shown in (c).

3e, implying that diffusion current rather than recombination current dominates the rectifying behavior. The diode exhibits a rectification factor of  $10^3$  under  $|V_{ds}| = 10$  V. To verify that rectifying behavior is originated from InSe/CuInSe<sub>2</sub> heterojunction,  $I$ – $V$  characteristics of individual multilayer InSe and thin-film CuInSe<sub>2</sub> nanosheets devices are measured. As shown in Figure 3f, the  $I$ – $V$  characteristics of multilayer InSe and thin-film CuInSe<sub>2</sub> nanosheets are totally different with InSe/CuInSe<sub>2</sub> heterojunction, and good linear  $I$ – $V$  characteristics can be observed in both InSe and CuInSe<sub>2</sub> nanosheet devices under low  $V_{ds}$  (as shown in Supporting Information Figure S1f). So the observed rectifying behavior reflects the intrinsic properties of InSe/CuInSe<sub>2</sub> heterojunction, forming a diode as expected from the band diagram.

**Broadband Photodetectors Based on InSe/CuInSe<sub>2</sub> Diodes.** As above mentioned, the optoelectronic properties of InSe/CuInSe<sub>2</sub> p–n heterojunction diode are measured using 2-probe structure without a Si gate. The photoresponse of the lateral InSe/CuInSe<sub>2</sub> heterojunction diode is investigated using different wavelength illumination or different optical intensities (shown in Figure 4). The InSe/CuInSe<sub>2</sub> lateral diode shows a broadband photoresponse ranging from ultraviolet (254 nm) to near-infrared light (850 nm) due to the small band gap of InSe and CuInSe<sub>2</sub> (Figure 4a). When biased in the reverse direction, the device is operated as a photodiode, which is a building block of photodetectors. The generated photocurrent  $I_{ph}$  ( $I_{ph} = I_{\text{illumination}} - I_{\text{dark}}$ ) varies with illumination wavelength. Specifically,  $I_{ph}$  increases from 1.7 nA at 850 nm light to 14.3 nA at 254 nm light with  $V_{ds} = -10$  V and illumination intensity of 0.29 mW cm<sup>−2</sup> (Figure 4b). The photocurrent increases with decreasing wavelength, because higher excitation energy

provided by higher photon energies can produce more excitons. The illumination intensity dependent photocurrent is investigated as shown in Figure 4c,d. The  $I_{ds}$ – $V_{ds}$  curve in Figure 4c shows that the  $I_{ph}$  rises with optical intensity from 0.29 mW cm<sup>−2</sup> to 0.70 mW cm<sup>−2</sup>. Furthermore, Figure 4d presents a linear relationship between the generated photocurrent  $I_{ph}$  and the optical intensity, indicating that the generated  $I_{ph}$  depends on the quantity of photogenerated carriers under optical illumination. Responsivity ( $R_\lambda$ ), one of key parameters for a photodetector,<sup>9</sup>  $R_\lambda$  can be calculated by the equation  $R_\lambda = I_{ph}/P_\lambda S$ , where  $I_{ph}$  is the generated photocurrent,  $P_\lambda$  is the incident optical intensity, and  $S$  is the effective illuminated area. Figure 4b,d show the calculated  $R_\lambda$  values under the illumination of various optical wavelengths and different optical intensities. The  $R_\lambda$  obtained at a bias voltage  $V_{ds} = -10$  V increases from 0.5 A W<sup>−1</sup> at the wavelength of 850 nm to 8.4 A W<sup>−1</sup> at the wavelength of 254 nm. A responsivity of 4.2 A W<sup>−1</sup> is obtained at the wavelength of 700 nm with the illumination power of 0.29 mW cm<sup>−2</sup> and a bias voltage of  $V_{ds} = -10$  V. With illumination optical intensity increasing, the responsivity decreases (Figure 4d). This reduction in photoresponsivity can be explained by the trap states existing at InSe/CuInSe<sub>2</sub> or at the interface between InSe/CuInSe<sub>2</sub> and the dielectric substrate. Moreover, we explore the impact of heterostructure film thickness on the photoresponse (shown in Supporting Information Figure S3e). Responsivity measured at the bias voltage of  $V_{ds} = -10$  V and at the wavelength of 700 nm with 0.29 mW cm<sup>−2</sup> power increases from 1.3 A W<sup>−1</sup> to 4.2 A W<sup>−1</sup> when InSe/CuInSe<sub>2</sub> film thickness varies from 20 to 40 nm due

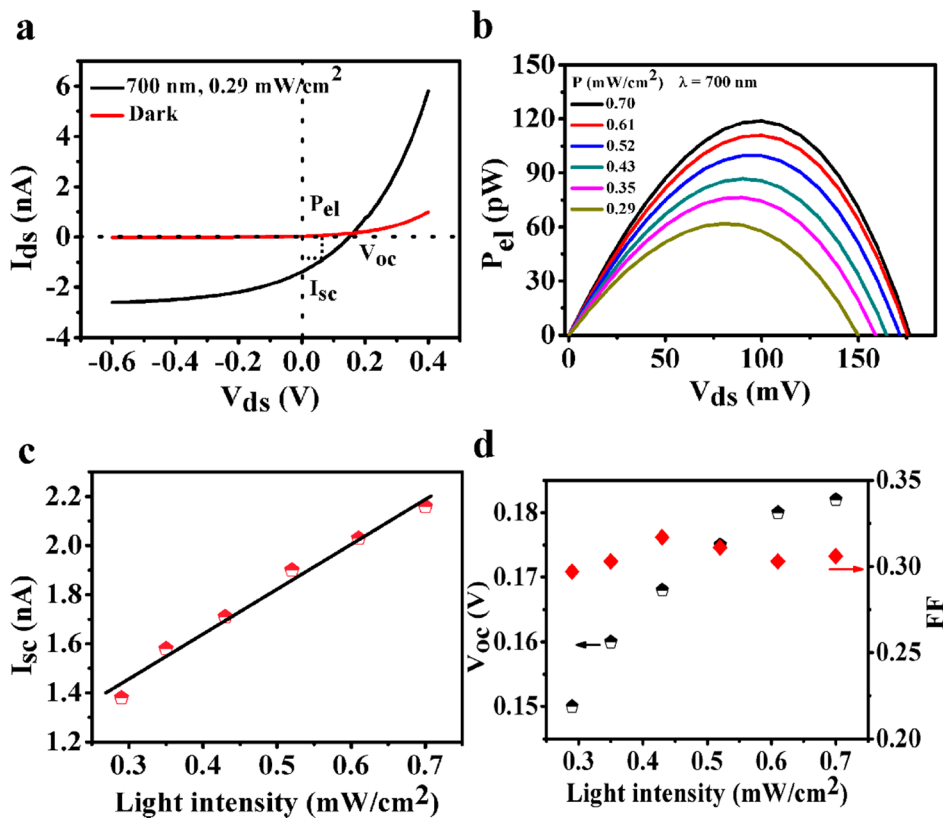


**Figure 5.** InSe/CuInSe<sub>2</sub> heterojunction as a solar cell. (a)  $I$ – $V$  characteristics of diode under 700 nm optical illumination of 0.29 mW cm<sup>−2</sup>. (b) Power ( $P_{el} = I_{ds}V_{ds}$ ) as a function of  $V_{ds}$  under various optical intensities. (c) Short-circuit current  $I_{sc}$  as a function of optical intensity. (d) Open-circuit voltage  $V_{oc}$  and fill factor (FF) as a function of optical intensity.

to the stronger photon absorption in thicker sheets (shown in Supporting Information Figure S3e).

**Photovoltaic Devices Based on Lateral InSe/CuInSe<sub>2</sub> Heterojunction.** In addition to photodetectors, the p–n diode is also the functional unit of solar cells. The capability of photovoltaic power generation of InSe/CuInSe<sub>2</sub> lateral diode is investigated. Figure 5a shows  $I_{ds}$ – $V_{ds}$  curves, which are measured in the dark and light conditions (700 nm light with power of 0.29 mW/cm<sup>2</sup>), respectively. Clearly, our lateral InSe/CuInSe<sub>2</sub> heterojunction diode shows an obvious photovoltaic effect and can be used for the photovoltaic solar energy conversion. The photovoltaic effect is attributed to InSe/CuInSe<sub>2</sub> p–n heterojunction diode (see more discussion in Supporting Information Figure S4). A zoomed-in view of  $I_{ds}$ – $V_{ds}$  curves in Figure 5a is used for the quadrant of photovoltaic power generation. The short-circuit  $I_{sc}$ , open-circuit voltage  $V_{oc}$ , and electrical power  $P_{el}$  ( $P_{el} = I_{ds}V_{ds}$ ) can be extracted. A peak value of  $P_{el,m} = 62$  pW is obtained at  $V_{ds} = 0.08$  V, and the corresponding current is  $I_{ds} = -0.77$  nA. The plots of  $P_{el}$  vs bias voltage at various optical intensities are presented in Figure 5b. The photovoltaic power generation presents a linear dependence on the optical intensity (Supporting Information Figure S5), and the value is as high as 120 pW when the optical intensity increases to 0.7 mW cm<sup>−2</sup>. The fill factor (FF), defined as the ratio of maximum  $P_{el,m}$  to  $I_{sc}$  and  $V_{oc}$  ( $FF = P_{el,m}/(I_{sc}V_{oc})$ ), is calculated to be 0.3. The power conversion effective ( $\eta_{pv} = P_{el,m}/P_{opt}$ ) of the device is defined as the capability of optical power converted to electrical power, where  $P_{opt}$  is the illumination optical power. In our case,  $\eta_{pv} = 3.5\%$  is obtained. As shown in Figure 5c, the  $I_{sc}$  shows a good linear relationship with  $P_{opt}$ . The  $V_{oc}$  exhibits a linear dependence on

$\ln(P_{opt})$  as presented in Figure 5d, and the FF is almost independent of the optical intensity (shown in Figure 5d). Furthermore, we investigate the photovoltaic efficiency as a function of InSe/CuInSe<sub>2</sub> heterojunction thickness (Supporting Information Figure S3f), and the power conversion effective  $\eta_{pv}$  varies from 1.2% to 3.5% as the layer thickness increases from 20 to 40 nm.

## CONCLUSION

In summary, we have demonstrated the successful fabrication of lateral p–n heterojunction diode in thin-film InSe/CuInSe<sub>2</sub> nanosheet by simple solid-state reaction. This chemical doping process is a facile operation and is more compatible with thin film manufacturing technology than previously used electrostatic tuning within the two-gate device configuration. The lateral InSe/CuInSe<sub>2</sub> p–n diode exhibits robust rectifying behavior with ideality factors of  $n = 1.3$  and a rectification factor of  $10^3$ . Lateral InSe/CuInSe<sub>2</sub> p–n diode based photodetectors and photovoltaic devices show a high photoresponsivity of 4.2 A W<sup>−1</sup> and relatively high power conversion efficiency of 3.5%. Such superior performance of our InSe/CuInSe<sub>2</sub> p–n diode can be attributed to the selection of direct band gap materials and high optical absorption with increased channel thickness. Our results demonstrate the exciting application potential of lateral InSe/CuInSe<sub>2</sub> p–n heterojunction diode for novel electronic and optoelectronic applications.

## ■ ASSOCIATED CONTENT

### Supporting Information

Electrical characterization of FETs based on InSe and CuInSe<sub>2</sub> nanosheets, AFM image and height profile of InSe/CuInSe<sub>2</sub> devices, electrical characterization of thinner (11 nm) InSe/CuInSe<sub>2</sub> diode, AFM surface morphology of thinner CuInSe<sub>2</sub> nanosheets and power conversion efficiency dependence on channel thickness, optoelectronic characterizations of InSe and CuInSe<sub>2</sub> devices, and photovoltaic power generation showing linear dependence on illumination light intensity. This material is available free of charge via the Internet at <http://pubs.acs.org/>.

## ■ AUTHOR INFORMATION

### Corresponding Author

\*E-mail: hupa@hit.edu.cn.

### Notes

The authors declare no competing financial interest.

## ■ ACKNOWLEDGMENTS

This work is supported by the National Natural Science Foundation of China (NSFC, No. 61172001, 21373068, 21303030) and the National key Basic Research Program of China (973 Program) under Grant 2013CB632900.

## ■ REFERENCES

- (1) Novoselov, K. S.; Jiang, D.; Schedin, F.; Booth, T. J.; Khotkevich, V. V.; Morozov, S. V.; Geim, A. K. *Proc. Natl. Acad. Sci. U. S. A.* **2005**, *102*, 10451.
- (2) Podzorov, V.; Gershenson, M.; Kloc, C.; Zeis, R.; Bucher, E. *Appl. Phys. Lett.* **2004**, *84*, 3301.
- (3) Fang, H.; Chuang, S.; Chang, T. C.; Takei, K.; Takahashi, T.; Javey, A. *Nano Lett.* **2012**, *12*, 3788.
- (4) Mudd, G. W.; Svatek, S. A.; Ren, T.; Patane, A.; Makarovskiy, O.; Eaves, L.; Beton, P. H.; Kovalyuk, Z. D.; Lashkarev, G. V.; Kudrynskyi, Z. R.; Dmitriev, A. I. *Adv. Mater.* **2013**, *25*, 5714.
- (5) Srinivasa, T. R.; Lu, Y.-Y.; U, R. K.; Sankar, R.; Liao, C.-D.; B, K. M.; Cheng, C.-H.; Chou, F. C.; Chen, Y.-T. *Nano Lett.* **2014**, *14*, 2800.
- (6) Li, L.; Yu, Y.; Ye, G. J.; Ge, Q.; Ou, X.; Wu, H.; Feng, D.; Chen, X. H.; Zhang, Y. *Nat. Nanotechnol.* **2014**, *9*, 372.
- (7) Liu, H.; Neal, A. T.; Zhu, Z.; Luo, Z.; Xu, X. F.; Tomanek, D.; Ye, P. D. D. *ACS Nano* **2014**, *8*, 4033.
- (8) Jariwala, D.; Sangwan, V. K.; Lauhon, L. J.; Marks, T. J.; Hersam, M. C. *ACS Nano* **2014**, *8*, 1102.
- (9) Yin, Z.; Li, H.; Li, H.; Jiang, L.; Shi, Y.; Sun, Y.; Lu, G.; Zhang, Q.; Chen, X.; Zhang, H. *ACS Nano* **2012**, *6*, 74.
- (10) Lopez-Sanchez, O.; Lembeck, D.; Kayci, M.; Radenovic, A.; Kis, A. *Nat. Nanotechnol.* **2013**, *8*, 497.
- (11) Zhang, W.; Chiu, M.-H.; Chen, C.-H.; Chen, W.; Li, L.-J.; Wee, A. T. S. *ACS Nano* **2014**, *8*, 8653.
- (12) Chang, Y.-H.; Zhang, W.; Zhu, Y.; Han, Y.; Pu, J.; Chang, J.-K.; Hsu, W.-T.; Huang, J.-K.; Hsu, C.-L.; Chiu, M.-H. *ACS Nano* **2014**, *8*, 8582.
- (13) Hu, P.; Wen, Z.; Wang, L.; Tan, P.; Xiao, K. *ACS Nano* **2012**, *6*, 5988.
- (14) Hu, P.; Wang, L.; Yoon, M.; Zhang, J.; Feng, W.; Wang, X.; Wen, Z.; Idrobo, J. C.; Miyamoto, Y.; Geohegan, D. B. *Nano Lett.* **2013**, *13*, 1649.
- (15) Lei, S.; Ge, L.; Najmaei, S.; George, A.; Kappera, R.; Lou, J.; Chhowalla, M.; Yamaguchi, H.; Gupta, G.; Vajtai, R. *ACS Nano* **2014**, *8*, 1263.
- (16) Buscema, M.; Groenendijk, D. J.; Blanter, S. I.; Steele, G. A.; van der Zant, H. S. J.; Castellanos-Gomez, A. *Nano Lett.* **2014**, *14*, 3347.
- (17) Zhang, Y.; Ye, J.; Yomogida, Y.; Takenobu, T.; Iwasa, Y. *Nano Lett.* **2013**, *13*, 3023.
- (18) Lee, C.-H.; Lee, G.-H.; M. van der Zande, A.; Chen, W.; Li, Y.; Han, M.; Cui, X.; Arefe, G.; Nuckolls, C.; F. Heinz, T.; Guo, J.; Hone, J.; Kim, P. *Nat. Nanotechnol.* **2014**, *9*, 676.
- (19) Furchi, M. M.; Pospischil, A.; Libisch, F.; Burgdörfer, J.; Mueller, T. *Nano Lett.* **2014**, *14*, 4785.
- (20) Deng, Y. X.; Luo, Z.; Conrad, N. J.; Liu, H.; Gong, Y. J.; Najmaei, S.; Ajayan, P. M.; Lou, J.; Xu, X. F.; Ye, P. D. *ACS Nano* **2014**, *8*, 8292.
- (21) Esmaeili-Rad, M. R.; Salahuddin, S. *Sci. Rep.* **2013**, *3*, 2345.
- (22) Jariwala, D.; Sangwan, V. K.; Wu, C. C.; Prabhmirashi, P. L.; Geier, M. L.; Marks, T. J.; Lauhon, L. J.; Hersam, M. C. *Proc. Natl. Acad. Sci. U. S. A.* **2013**, *110*, 18076.
- (23) Bernardi, M.; Palummo, M.; Grossman, J. C. *Nano Lett.* **2013**, *13*, 3664.
- (24) Zhang, W.; Chuu, C.-P.; Huang, J.-K.; Chen, C.-H.; Tsai, M.-L.; Chang, Y.-H.; Liang, C.-T.; Chen, Y.-Z.; Chueh, Y.-L.; He, J.-H. *Sci. Rep.* **2014**, *4*, 3826.
- (25) Baugher, B. W. H.; Churchill, H. O. H.; Yang, Y. F.; Jarillo-Herrero, P. *Nat. Nanotechnol.* **2014**, *9*, 262.
- (26) Pospischil, A.; Furchi, M. M.; Mueller, T. *Nat. Nanotechnol.* **2014**, *9*, 257.
- (27) Buscema, M.; Groenendijk, D. J.; Steele, G. A.; van der Zant, H. S.; Castellanos-Gomez, A. *Nat. Commun.* **2014**, *5*, 4651.
- (28) Huang, C.; Wu, S.; M. Sanchez, A.; J. P. Peters, J.; Beanland, R.; S. Ross, J.; Rivera, P.; Yao, W.; H. Cobden, D.; Xu, X. *Nat. Mater.* **2014**, *13*, 1096.
- (29) Kuroda, N.; Nishina, Y. *Solid State Commun.* **1980**, *34*, 481.
- (30) Imai, K.; Suzuki, K.; Haga, T.; Hasegawa, Y.; Abe, Y. *J. Cryst. Growth* **1981**, *54*, 501.
- (31) Rockett, A.; Birkmire, R. W. *J. Appl. Phys.* **1991**, *70*, R81.
- (32) Schoen, D. T.; Peng, H. L.; Cui, Y. *ACS Nano* **2013**, *7*, 3205.
- (33) Tao, X.; Mafi, E.; Gu, Y. *J. Phys. Chem. Lett.* **2014**, *5*, 2857.
- (34) Schoen, D. T.; Peng, H. L.; Cui, Y. *J. Am. Chem. Soc.* **2009**, *131*, 7973.
- (35) Hsin, C. L.; Lee, W. F.; Huang, C. T.; Huang, C. W.; Wu, W. W.; Chen, L. J. *Nano Lett.* **2011**, *11*, 4348.
- (36) Srinivasa, T. R.; Lu, Y.-Y.; U, R. K.; Sankar, R.; Liao, C.-D.; Cheng, C.-H.; Chou, F. C.; Chen, Y.-T. *Nano Lett.* **2014**, *14*, 2800.
- (37) Feng, W.; Zheng, W.; Cao, W.; Hu, P. *Adv. Mater.* **2014**, *26*, 6587.
- (38) Choi, M. S.; Qu, D.; Lee, D.; Liu, X.; Watanabe, K.; Taniguchi, T.; Yoo, W. J. *ACS Nano* **2014**, *8*, 9332.
- (39) Rincon, C.; Ramirez, F. *J. Appl. Phys.* **1992**, *72*, 4321.